

Measurement of $ep \rightarrow e' p \pi^+ \pi^-$: experimental procedures and baryon resonance analysis

M. Ripani,¹ V.D. Burkert,² V. Mokeev,³ M. Battaglieri,¹ R. De Vita,¹ E. Golovach,³ M. Taiuti,¹
 G. Adams,³⁰ E. Anciant,⁸ M. Anghinolfi,¹ B. Asavapibhop,²³ G. Audit,⁸ T. Auger,⁸ H. Avakian,^{2,17}
 H. Bagdasaryan,³⁸ J.P. Ball,⁴ S. Barrow,¹⁴ K. Beard,²⁰ M. Bektasoglu,²⁷ B.L. Berman,¹⁵ N. Bianchi,¹⁷
 A.S. Biselli,³⁰ S. Boiarinov,^{2,19} B.E. Bonner,³¹ S. Bouchigny,^{18,2} R. Bradford,⁶ D. Branford,¹² W.J. Briscoe,¹⁵
 W.K. Brooks,² J.R. Calarco,²⁴ D.S. Carman,²⁶ B. Carnahan,⁷ A. Cazes,³³ C. Cetina,¹⁵ L. Ciciani,²⁷
 P.L. Cole,^{34,2} A. Coleman,³⁷ D. Cords,² P. Corvisiero,¹ D. Crabb,³⁶ H. Crannell,⁷ J.P. Cummings,³⁰
 E. De Sanctis,¹⁷ P.V. Degtyarenko,² H. Denizli,²⁸ L. Dennis,¹⁴ K.V. Dharmawardane,²⁷ C. Djalali,³³
 G.E. Dodge,²⁷ D. Doughty,^{9,2} P. Dragovitsch,¹⁴ M. Dugger,⁴ S. Dytman,²⁸ M. Eckhause,³⁷ H. Egiyan,³⁷
 K.S. Egiyan,³⁸ L. Elouadrhiri,² A. Empl,³⁰ R. Fatemi,³⁶ G. Fedotov,³ G. Feldman,¹⁵ R.J. Feuerbach,⁶
 J. Ficencic,³⁵ T.A. Forest,²⁷ H. Funsten,³⁷ S.J. Gaff,¹¹ M. Gai,¹⁰ M. Garçon,⁸ G. Gavalian,^{24,38} S. Gilad,²²
 G.P. Gilfoyle,³² K.L. Giovanetti,²⁰ P. Girard,³³ K. Griffioen,³⁷ M. Guidal,¹⁸ M. Guillo,³³ L. Guo,²
 V. Gyurjyan,² C. Hadjidakis,¹⁸ J. Hardie,^{9,2} D. Heddle,^{9,2} P. Heimberg,¹⁵ F.W. Hersman,²⁴ K. Hicks,²⁶
 R.S. Hicks,²³ M. Holtrop,²⁴ J. Hu,³⁰ C.E. Hyde-Wright,²⁷ B. Ishkhanov,³ M.M. Ito,² D. Jenkins,³⁵ K. Joo,^{2,36}
 J.H. Kelley,¹¹ J.D. Kellie,¹⁶ M. Khandaker,²⁵ K.Y. Kim,²⁸ K. Kim,²¹ W. Kim,²¹ A. Klein,²⁷ F.J. Klein,^{7,2}
 A.V. Klimenko,²⁷ M. Klusman,³⁰ M. Kossov,¹⁹ L.H. Kramer,^{13,2} Y. Kuang,³⁷ S.E. Kuhn,²⁷ J. Kuhn,³⁰
 J. Lachniet,⁶ J.M. Laget,⁸ D. Lawrence,²³ Ji Li,³⁰ K. Livingston,¹⁶ A. Longhi,⁷ K. Lukashin,² J.J. Manak,²
 C. Marchand,⁸ S. McAleer,¹⁴ J. McCarthy,³⁶ J.W.C. McNabb,⁶ B.A. Mecking,² M.D. Mestayer,² C.A. Meyer,⁶
 K. Mikhailov,¹⁹ R. Minehart,³⁶ M. Mirazita,¹⁷ R. Miskimen,²³ L. Morand,⁸ S.A. Morrow,¹⁸ M.U. Mozer,²⁶
 V. Muccifora,¹⁷ J. Mueller,²⁸ L.Y. Murphy,¹⁵ G.S. Mutchler,³¹ J. Napolitano,³⁰ R. Nasseripour,¹³ S.O. Nelson,¹¹
 S. Niccolai,¹⁵ G. Niculescu,²⁶ I. Niculescu,¹⁵ B.B. Niczyporuk,² R.A. Niyazov,² M. Nozar,^{2,25} G.V. O'Rielly,¹⁵
 A.K. Opper,²⁶ M. Osipenko,³ K. Park,²¹ E. Pasyuk,⁴ G. Peterson,²³ S.A. Philips,¹⁵ N. Pivnyuk,¹⁹ D. Pocanic,³⁶
 O. Pogorelko,¹⁹ E. Polli,¹⁷ S. Pozdniakov,¹⁹ B.M. Freedom,³³ J.W. Price,⁵ Y. Prok,³⁶ D. Protopopescu,²⁴
 L.M. Qin,²⁷ B. Quinn,⁶ B.A. Raue,^{13,2} G. Riccardi,¹⁴ G. Ricco,¹ B.G. Ritchie,⁴ F. Ronchetti,^{17,29}
 P. Rossi,¹⁷ D. Rowntree,²² P.D. Rubin,³² F. Sabatié,^{8,27} K. Sabourov,¹¹ C. Salgado,²⁵ J.P. Santoro,^{35,2}
 V. Sapunenko,¹ R.A. Schumacher,⁶ V.S. Serov,¹⁹ A. Shafi,¹⁵ Y.G. Sharabian,^{2,38} J. Shaw,²³ S. Simionatto,¹⁵
 A.V. Skabelin,²² E.S. Smith,² L.C. Smith,³⁶ D.I. Sober,⁷ M. Spraker,¹¹ A. Stavinsky,¹⁹ S. Stepanyan,^{27,38}
 P. Stoler,³⁰ I.I. Strakovsky,¹⁵ S. Taylor,³¹ D.J. Tedeschi,³³ U. Thoma,² R. Thompson,²⁸ L. Todor,⁶
 M. Ungaro,³⁰ M.F. Vineyard,³² A.V. Vlassov,¹⁹ K. Wang,³⁶ L.B. Weinstein,²⁷ H. Weller,¹¹ D.P. Weygand,²
 C.S. Whisnant,³³ E. Wolin,² M.H. Wood,³³ A. Yegneswaran,² J. Yun,²⁷ B. Zhang,²² J. Zhao,²² Z. Zhou,²²

¹ INFN, Sezione di Genova, 16146 Genova, Italy

² Thomas Jefferson National Accelerator Facility, Newport News, Virginia 23606

³ Moscow State University, 119899 Moscow, Russia

⁴ Arizona State University, Tempe, Arizona 85287

⁵ University of California at Los Angeles, Los Angeles, California 90095

⁶ Carnegie Mellon University, Pittsburgh, Pennsylvania 15213

⁷ Catholic University of America, Washington, D.C. 20064

⁸ CEA-Saclay, Service de Physique Nucléaire, F91191 Gif-sur-Yvette, Cedex, France

⁹ Christopher Newport University, Newport News, Virginia 23606

¹⁰ University of Connecticut, Storrs, Connecticut 06269

¹¹ Duke University, Durham, North Carolina 27708

¹² Edinburgh University, Edinburgh EH9 3JZ, United Kingdom

¹³ Florida International University, Miami, Florida 33199

¹⁴ Florida State University, Tallahassee, Florida 32306

¹⁵ The George Washington University, Washington, DC 20052

¹⁶ University of Glasgow, Glasgow G12 8QQ, United Kingdom

¹⁷ INFN, Laboratori Nazionali di Frascati, PO 13, 00044 Frascati, Italy

¹⁸ Institut de Physique Nucleaire ORSAY, IN2P3 BP 1, 91406 Orsay, France

¹⁹ Institute of Theoretical and Experimental Physics, Moscow, 117259, Russia

²⁰ James Madison University, Harrisonburg, Virginia 22807

²¹ Kyungpook National University, Daegu 702-701, South Korea

²² Massachusetts Institute of Technology, Cambridge, Massachusetts 02139

²³ University of Massachusetts, Amherst, Massachusetts 01003

²⁴ University of New Hampshire, Durham, New Hampshire 03824

²⁵ Norfolk State University, Norfolk, Virginia 23504

²⁶ Ohio University, Athens, Ohio 45701

²⁷ Old Dominion University, Norfolk, Virginia 23529

²⁸ *University of Pittsburgh, Pittsburgh, Pennsylvania 15260*

²⁹ *Universita' di ROMA III, 00146 Roma, Italy*

³⁰ *Rensselaer Polytechnic Institute, Troy, New York 12180*

³¹ *Rice University, Houston, Texas 77005*

³² *University of Richmond, Richmond, Virginia 23173*

³³ *University of South Carolina, Columbia, South Carolina 29208*

³⁴ *University of Texas at El Paso, El Paso, Texas 79968*

³⁵ *Virginia Polytechnic Institute and State University, Blacksburg, Virginia 24061*

³⁶ *University of Virginia, Charlottesville, Virginia 22901*

³⁷ *College of William and Mary, Williamsburg, Virginia 23187 and*

³⁸ *Yerevan Physics Institute, 375036 Yerevan, Armenia*

(Dated: October 31, 2018)

The cross section for the reaction $ep \rightarrow e'p\pi^+\pi^-$ was measured in the resonance region for $1.4 < W < 2.1$ GeV and $0.5 < Q^2 < 1.5$ GeV²/c² using the CLAS detector at Jefferson Laboratory. The data show resonant structures not visible in previous experiments. The comparison of our data to a phenomenological prediction using available information on N^* and Δ states shows an evident discrepancy. A better description of the data is obtained either by a sizeable change of the properties of the $P_{13}(1720)$ resonance or by introducing a new baryon state, not reported in published analyses.

PACS numbers: 13.60.Le, 13.40.Gp, 14.20.Gk

Electromagnetic excitation of nucleon resonances is sensitive to the spin and spatial structure of the transition, which in turn is connected to fundamental properties of baryon structure, like spin-flavor symmetries, confinement, and effective degrees of freedom. In the mass region above 1.6 GeV, many overlapping baryon states are present, and some of them are not well known; measurement of the transition form factors of these states is important for our understanding of the internal dynamics of baryons. Many of these high-mass excited states tend to decouple from the single-meson channels and to decay predominantly into multi-pion channels, such as $\Delta\pi$ or $N\rho$, leading to $N\pi\pi$ final states [1]. Moreover, quark models with approximate (or “broken”) SU(6) \otimes O(3) symmetry [2, 3] predict more states than have been found experimentally; QCD mixing effects could decouple these unobserved states from the pion-nucleon channel [2] while strongly coupling them to two-pion channels [2, 4, 5]. These states would therefore not be observable in reactions with πN in the initial or final state. Other models, with different symmetry properties and a reduced number of degrees of freedom, as e.g. in ref. [6], predict fewer states. Experimental searches for at least some of the “missing” states predicted by the symmetric quark models, which are not predicted by models using alternative symmetries, are crucial in discriminating between these models. Electromagnetic amplitudes for some missing states are predicted to be sizeable [2] as well. Therefore, exclusive double-pion electroproduction is a fundamental tool in measuring poorly known states and possibly observing new ones.

In this paper we report a measurement of the $ep \rightarrow e'p\pi^+\pi^-$ reaction studied with the CEBAF Large Acceptance Spectrometer (CLAS) at Jefferson Lab. CLAS consists of a six-coil superconducting magnet producing an approximately toroidal magnetic field, allowing detection of electrons and hadrons and full 4-momentum reconstruction. Three sets of drift chambers allow the de-

termination of the momenta of the charged particles with polar angles from 10° to 140°. A complete coverage of scintillators allows the discrimination of particles by a time-of-flight technique described in ref. [7]. The magnetic field was set to bent positive particles outwards, away from the primary beam. We analyzed data taken in the so-called ‘elc’ running period, corresponding to about two months of data taking in the spring of 1999. Beam currents of a few nA were delivered to Hall B on a liquid-hydrogen target, corresponding to luminosities up to 4×10^{33} cm⁻²s⁻¹. The beam energies selected for this analysis were: 2.567 GeV at a torus current of 1500 A (‘low’ field), with the goal of obtaining two Q^2 bins, between 0.5 and 0.8 GeV²/c² and between 0.8 and 1.1 GeV²/c², with W up to 1.9 GeV; 4.247 GeV at a field of 2250 A (‘low’ field), to obtain Q^2 between 1.1 and 1.5 GeV²/c², with W up to 2.1 GeV. Important features of the CLAS [8] are its large kinematic coverage for multi-charged-particle final states and its good momentum resolution ($\Delta p/p \sim 1\%$). Using an inclusive electron trigger, many exclusive hadronic final states were measured simultaneously. Scattered electrons were identified through cuts on the calorimeter energy loss and the Cherenkov photo-electron distribution. Different channels were separated through particle identification using time-of-flight information and other kinematic cuts.

The hardware trigger in CLAS was based on a coincidence between Cherenkov counter and electromagnetic forward calorimeter. The discriminator threshold in the Cherenkov was put at a signal level of less than a single photoelectron produced on the photocathode, to avoid losing good events while rejecting most of the pion background. The energy threshold in the calorimeter was set to cut off events as close as possible to the kinematic edges of the W and Q^2 domain covered by the measurement, but sufficiently high to keep the low energy contamination due to hadronically interacting particles at a reasonable limit. A cut on the energy deposited in the

calorimeter was applied to eliminate part of the remaining pion background, mostly due to knock-off electrons giving a signal in the Cherenkov counter. We studied the effect of this cut on the electron detection efficiency, deriving a correction that was applied to the data. The Cherenkov efficiency was also studied by means of the shape of the photoelectron distribution in each module. This way, we evaluated the effect of a cut on the photoelectron number on the electron detection efficiency on each single Cherenkov module, as well as the module-to-module uniformity, deriving the appropriate corrections to be applied to the data.

Another cut was applied in the β versus momentum plot, to select pions and protons in the reaction analyzed. All Time of Flight (ToF) scintillator paddles were carefully inspected to make sure that the cut applied was appropriate for all of them. To identify the $e'p\pi^+\pi^-$ final state, we used the missing-mass technique, requiring detection in CLAS of at least $ep\pi^+$. The good resolution allowed selection of the exclusive final state, $ep\pi^+\pi^-$. After applying all cuts, our data sample included about 2×10^5 two-pion events. Fig. 1 shows the missing mass distribution obtained from CLAS, together with the applied cut. The tail at higher mass is due to radiative effects and to multiple pion production.

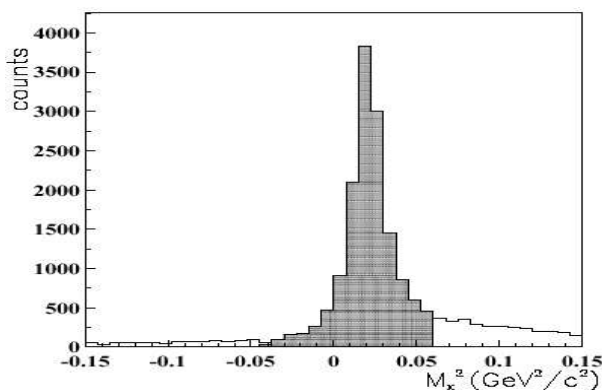


FIG. 1: Missing mass for detection of $ep\pi^+$, at $W=1.6-1.7$ GeV and at $Q^2=0.5-0.8$ $(\text{GeV}/c)^2$. The tail at higher mass is due to radiative effects and to multiple pion production. The hatched area represents the adopted cut.

In order to check the stability of CLAS in the detection of different reactions, we defined a set of histograms representing various reaction yields, i.e. electron inclusive, electron-proton inclusive, electron elastic (W cut), electron-proton elastic (W plus θ - ϕ correlation cut), electron-proton from the Δ (W cut) and finally electron-proton- π^+ with a cut on the missing π^- , each single yield being normalised to the Faraday cup charge obtained from the so called “live-gated” signal, where the signal from the Faraday cup is only integrated during the live-time: this way, the charge is already corrected for the data acquisition dead-time. Such normalised yields were calculated, using the PID procedures described in the previous subsection, for each data file inside a run

(a run being typically a data taking over a period of an hour), therefore providing a very accurate monitoring of stability even inside a single run. “Good files” were selected requiring that the normalised yield for a single file should not deviate more than a few percent from the average. Subsequent analysis was performed only on the good files.

To obtain the cross section from the raw data, it is necessary to correct for detector non-uniformity, which has origin both in the geometry and in the response of the equipment to different particles. The geometrical and kinematic non-uniformity can be very well described by means of fiducial cuts that describe regions of the detector where the response of the various subsystems is well known. Fiducial cuts will eliminate dead regions like the torus coils in the first place. The detector response inside the fiducial regions was simulated using a GEANT-based representation of the detector containing a detailed description of particle interaction with the various subsystems. To evaluate all detector corrections, we divided the particle yield into kinematic bins defined through a complete set of independent kinematic variables of the hadronic state, plus W and Q^2 . This corresponds to binning all four-momenta of the particles involved (with the exception of the electron, for which no binning is applied to ϕ azimuthal angle for symmetry reasons). This way, the folding of the detector response to the cross sections is done in narrow kinematic regions, where the cross section variation will be limited. The dependence of the results on the assumed particle distributions will therefore be much reduced. However, events still have to be generated according to a realistic Monte Carlo, in order to minimize the model dependence of acceptance and efficiency.

The event generator used for simulations in this experiment contains several electroproduction cross sections, including single, double and triple pion electroproduction. The code relies on cross section tables that describe measured total and differential cross sections from the literature, scaled by a virtual photon flux and a dipole form factor to provide a reasonable fall off with Q^2 . Therefore our code gives a realistic description of cross sections and their relative weights, as well as backgrounds generated from competing channels. Radiative effects were also included in the simulation. As an example of how the Monte Carlo reproduces the main features seen in the data, we reproduce here the comparison of some kinematic distributions from the data at 2.567 GeV beam energy, 1500 A field, with the corresponding simulation. As specific example we report the case of the W bin 1.6-1.625 GeV, and Q^2 between 0.5 and 0.8 GeV^2/c^2 . Figure 2 shows the invariant mass distribution for the pion-pion pair. Figure 3 shows the invariant mass distribution for the proton- π^+ pair. Figure 4 shows the CM angle of the $p-\pi^-$ pair (which would correspond to the CM angle of a Δ^0 in the specific case that a Δ^0 is produced).

A particularly important issue regards the percentage of events lost in the binning process due to bins with zero

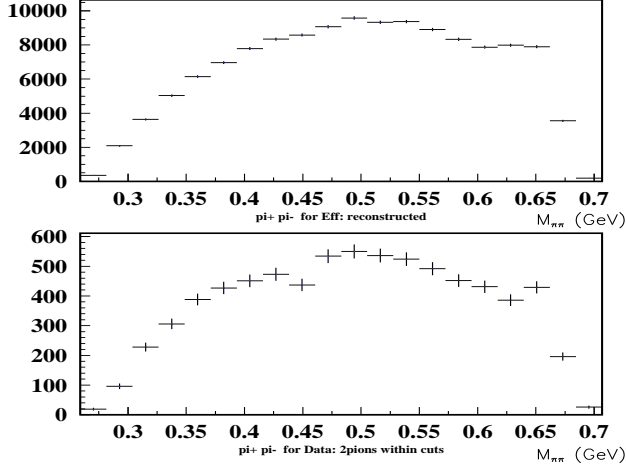


FIG. 2: Simulated (top) and measured (bottom) invariant mass for the pion-pion pair, when detecting $ep\pi^+$, at 2.567 GeV beam energy, 1500 A field, W between 1.6 and 1.625 GeV and Q^2 between 0.5 and 0.8 GeV^2/c^2 .

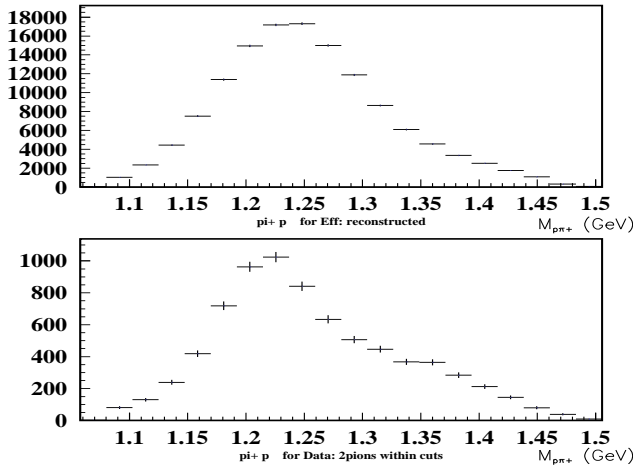


FIG. 3: Simulated (top) and measured (bottom) invariant mass for the proton- π^+ pair, when detecting $ep\pi^+$, at 2.567 GeV beam energy, 1500 A field, W between 1.6 and 1.625 GeV and Q^2 between 0.5 and 0.8 GeV^2/c^2 .

acceptance: of course, for such bins it is not possible to correct the data and obtain a cross section; being the kinematic variable space multidimensional in the case of double pion production, extrapolating the cross sections from neighboring bins with non-zero acceptance to bins with zero acceptance can be unreliable. Therefore, we checked carefully, using our realistic Monte Carlo, the percentage of cross section lost because of bins with zero acceptance. It turned out that with the adopted binning, the percentage of unmeasured cross section in bins with vanishing acceptance was below 10 % and typically of the order of a few percent. Actually, the fact that a cell has zero acceptance or efficiency may be just connected to insufficient statistics in the simulation, as many cells end up with very few generated events; nevertheless, for those cells it is not possible to perform a correction to the data.

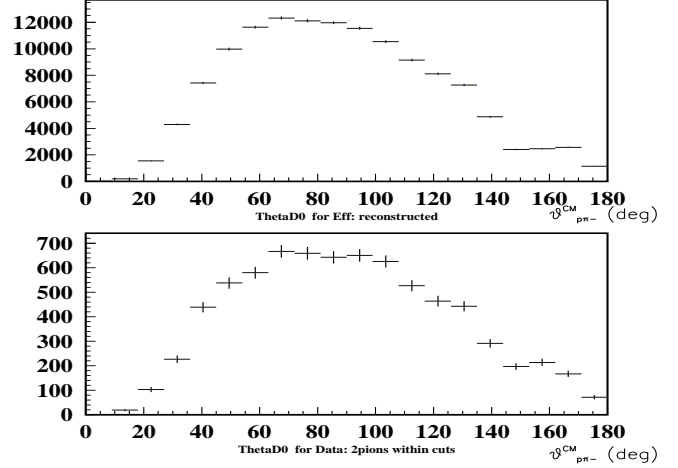


FIG. 4: Simulated (top) and measured (bottom) angular distribution of the $p-\pi^-$ pair in the CM system, when detecting $ep\pi^+$, at 2.567 GeV beam energy, 1500 A field, W between 1.6 and 1.625 GeV and Q^2 between 0.5 and 0.8 GeV^2/c^2 .

To get the final cross sections, we therefore performed an extrapolation to the empty bins using the MonteCarlo distributions as an estimate of the missing cross section. This extrapolation is typically only a few percent and we quoted as systematic error a quantity equal to one half of the extrapolation, assuming that the extrapolated cross section may be wrong by plus or minus 50 %, due to the assumptions in the MonteCarlo.

The range of invariant hadronic center-of-mass (CM) energy W (in 25 MeV bins) was 1.4-1.9 GeV for the first two bins in the invariant momentum transfer Q^2 , 0.5-0.8 $(\text{GeV}/c)^2$ and 0.8-1.1 $(\text{GeV}/c)^2$, and 1.4-2.1 GeV for the highest Q^2 bin, 1.1-1.5 $(\text{GeV}/c)^2$. Following the procedures schematically described above, data were corrected for acceptance, reconstruction efficiency, radiative effects, and empty target counts. They were further binned in the following set of hadronic CM variables: invariant mass of the $p\pi^+$ pair (10 bins), invariant mass of the $\pi^+\pi^-$ pair (10 bins), π^- polar angle θ (10 bins), azimuthal angle ϕ (5 bins), and rotation freedom ψ of the $p\pi^+$ pair with respect to the hadronic plane (5 bins). The fully differential cross section is of the form:

$$\frac{d\sigma}{dW dQ^2 dM_{p\pi^+} dM_{\pi^+\pi^-} d\cos\theta_{\pi^-} d\phi_{\pi^-} d\psi_{p\pi^+}} = \Gamma_v \frac{d\sigma_v}{dM_{p\pi^+} dM_{\pi^+\pi^-} d\cos\theta_{\pi^-} d\phi_{\pi^-} d\psi_{p\pi^+}} = \Gamma_v \frac{d\sigma_v}{d\tau} \quad (1)$$

$$\Gamma_v = \frac{\alpha}{4\pi} \frac{1}{E^2 M_p^2} \frac{W(W^2 - M_p^2)}{(1 - \epsilon)Q^2} \quad (2)$$

where Γ_v is the virtual photon flux, $\frac{d\sigma_v}{d\tau}$ is the virtual photon cross section, α is the fine structure constant, E is the electron beam energy, M_p is the proton mass, and ϵ is the virtual photon transverse polarization [9].

Since existing theoretical models [11] are limited to $W < 1.6$ GeV, we have employed a phenomenological

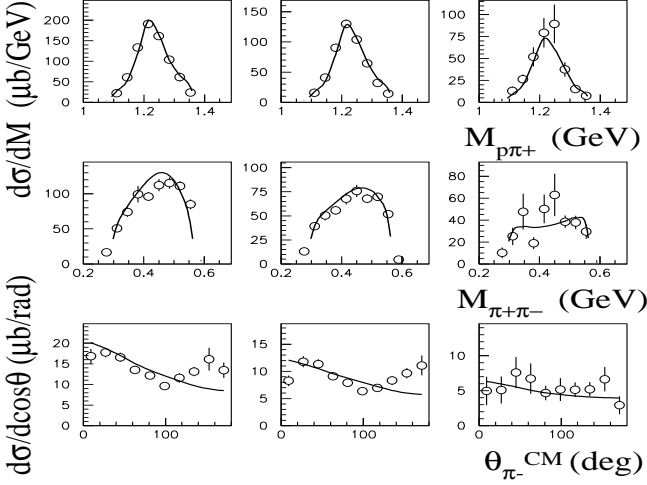


FIG. 5: $\frac{d\sigma_v}{dM_{p\pi^+}}$, $\frac{d\sigma_v}{dM_{\pi^+\pi^-}}$, and $\frac{d\sigma_v}{d\cos\theta_{\pi^-}}$ from CLAS (from top to bottom) at $W=1.5-1.525$ GeV and for the three mentioned Q^2 intervals (left to right). The error bars include statistical errors only. The curves represent our step (A) reference calculations.

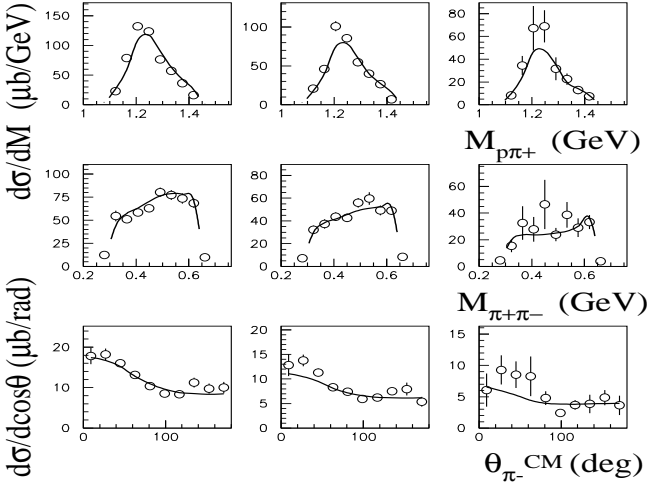


FIG. 6: $\frac{d\sigma_v}{dM_{p\pi^+}}$, $\frac{d\sigma_v}{dM_{\pi^+\pi^-}}$, and $\frac{d\sigma_v}{d\cos\theta_{\pi^-}}$ from CLAS (from top to bottom) at $W=1.575-1.6$ GeV and for the three mentioned Q^2 intervals (left to right). The error bars include statistical errors only. The curves represent our step (A) reference calculations.

calculation [12] for a first interpretation of the data. This model describes the reaction $\gamma_v p \rightarrow p\pi^+\pi^-$ in the kinematic range of interest as a sum of amplitudes for $\gamma_v p \rightarrow \Delta\pi \rightarrow p\pi^+\pi^-$ and $\gamma_v p \rightarrow \rho^0 p \rightarrow p\pi^+\pi^-$, while all other possible mechanisms are parameterized as phase space. A detailed treatment was developed for the non-resonant contributions to $\Delta\pi$, while for ρp production they were described through a diffractive ansatz. For the resonant part, a total of 12 states, classified as 4^* [1], with sizeable $\Delta\pi$ and/or ρp decays, were included based on a Breit-Wigner ansatz. A few model parameters in non-resonant production were fitted to CLAS data at high W , where the non-resonant part creates a forward peaking in the angular distributions, and kept fixed in the

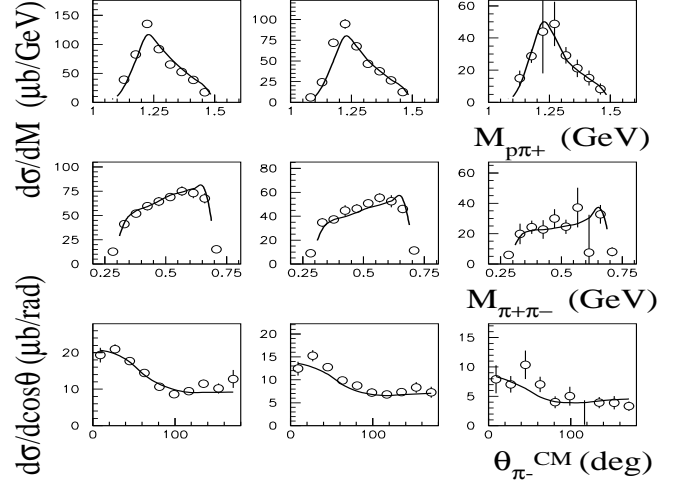


FIG. 7: $\frac{d\sigma_v}{dM_{p\pi^+}}$, $\frac{d\sigma_v}{dM_{\pi^+\pi^-}}$, and $\frac{d\sigma_v}{d\cos\theta_{\pi^-}}$ from CLAS (from top to bottom) at $W=1.625-1.65$ GeV and for the three mentioned Q^2 intervals (left to right). The error bars include statistical errors only. The curves represent our step (A) reference calculations.

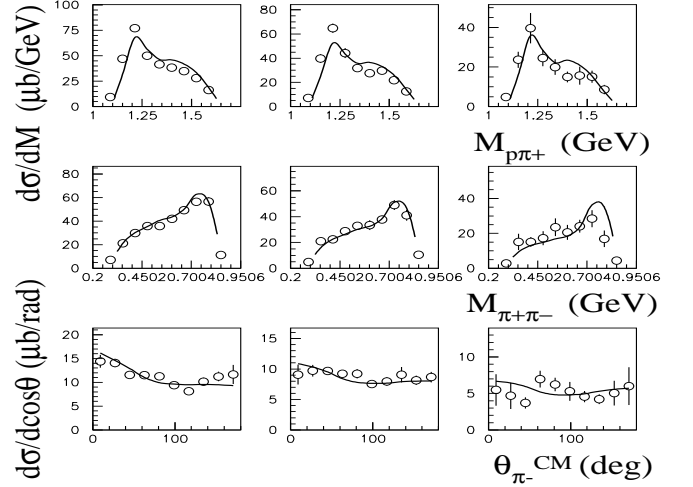


FIG. 8: $\frac{d\sigma_v}{dM_{p\pi^+}}$, $\frac{d\sigma_v}{dM_{\pi^+\pi^-}}$, and $\frac{d\sigma_v}{d\cos\theta_{\pi^-}}$ from CLAS (from top to bottom) at $W=1.775-1.8$ GeV and for the three mentioned Q^2 intervals (left to right). The error bars include statistical errors only. The curves represent our step (A) reference calculations.

subsequent analysis. The phase between resonant and non-resonant $\Delta\pi$ mechanisms was fitted to the CLAS data as well. To simplify the fits, we reduced eqn. (1) to three single-differential cross sections, $\frac{d\sigma}{dM_{p\pi^+}}$, $\frac{d\sigma}{dM_{\pi^+\pi^-}}$, and $\frac{d\sigma}{d\cos\theta_{\pi^-}}$, by integrating over the other hadronic variables. These three 1-D distributions were then fitted simultaneously. Here $\frac{d\sigma}{dM_{p\pi^+}}$ and $\frac{d\sigma}{d\cos\theta_{\pi^-}}$ are both connected with the dominant $\Delta^{++}\pi^-$ production reaction, while $\frac{d\sigma}{dM_{\pi^+\pi^-}}$ is connected with $\rho\rho^0$ production. For each W and Q^2 bin, a total of 26 data points from the three single-differential cross sections were used in our fits. The two edge points in both the $p\pi^+$ and $\pi^+\pi^-$ mass distributions were excluded as the model did not

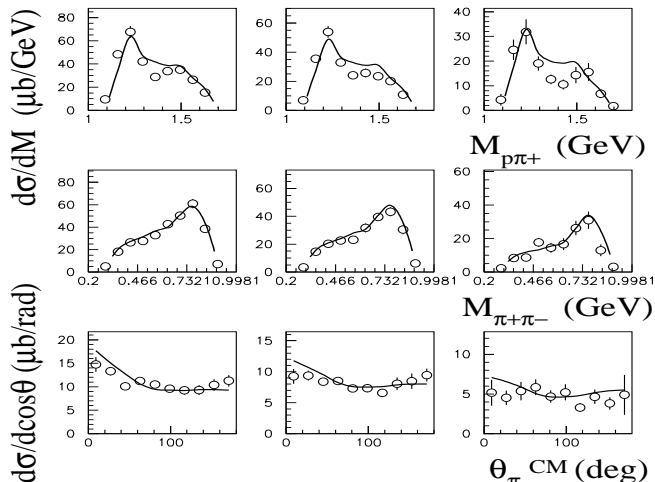


FIG. 9: $\frac{d\sigma_v}{dM_{p\pi^+}}$, $\frac{d\sigma_v}{dM_{\pi^+\pi^-}}$, and $\frac{d\sigma_v}{d\cos\theta_{\pi^-}}$ from CLAS (from top to bottom) at $W=1.825-1.85$ GeV and for the three mentioned Q^2 intervals (left to right). The error bars include statistical errors only. The curves represent our step (A) reference calculations.

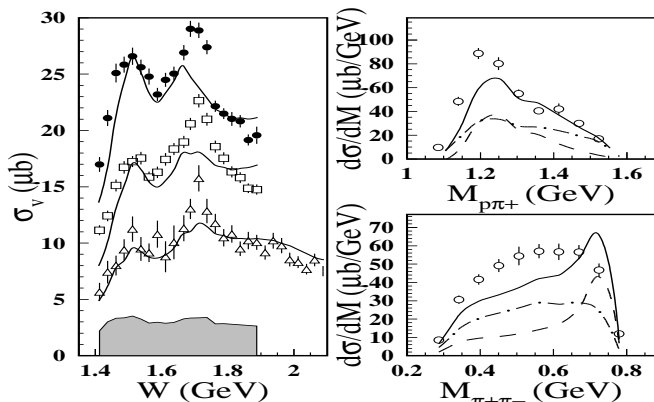


FIG. 10: Left: Total cross section for $\gamma_v p \rightarrow p\pi^+\pi^-$ as a function of W . Data from CLAS are shown at $Q^2=0.5-0.8$ (GeV/c^2) (full points), $Q^2=0.8-1.1$ (GeV/c^2) (open squares), and $Q^2=1.1-1.5$ (GeV/c^2) (open triangles). Error bars are statistical only, while the bottom band shows the systematic error for the lowest Q^2 bin. The curves represent our step (A) reference calculations. Right: $\frac{d\sigma_v}{dM_{\pi^+\pi^-}}$ from CLAS at $Q^2=0.8-1.1$ (GeV/c^2) and $W=1.7-1.725$ GeV (statistical error bars only). The curves represent our step (A) reference calculations, extrapolated to the edge points. The dashed line includes all resonances, the dot-dashed line includes only the non-resonant part, and the solid line is the full calculation.

take into account the kinematic smearing in the $M_{\pi^+\pi^-}$ versus $M_{p\pi^+}$ plot caused by the W bin width.

The physics analysis included the following steps: (A) We produced reference curves using the available information on the N^* and Δ resonances in 1.2-2 GeV mass range. Discrepancies between the CLAS data and our calculation were observed, which led to the subsequent steps B and C. (B) Data around $W=1.7$ GeV were fitted using the known resonances in the PDG but allowing

the resonance parameters to vary in a number of ways. The best fit, corresponding to a prominent P_{13} partial wave, could be attributed to the PDG $P_{13}(1720)$ resonance, but with parameters significantly modified from the PDG values. (C) As an alternative description, we introduced a new baryon state around 1.7 GeV. In what follows we describe each of the steps above in more detail.

Step (A) - To produce our reference curves, the Q^2 evolution of the $A_{1/2}$ and $A_{3/2}$ electromagnetic couplings for the states was taken either from parameterizations of existing data [13], or from Single Quark Transition Model (SQTm) fits [13] where no data were available. For the $P_{11}(1440)$ (Roper), given the scarce available data, the amplitude $A_{1/2}$ was taken from a Non-Relativistic Quark Model (NRQM) [14]. Partial LS decay widths were taken from a previous analysis of hadronic data [15] and renormalized to the total widths from Ref. [1]. Results from step (A) are reported in Figs. 5 to 9 for the specific one-dimensional differential cross sections analysed and for a sample of W bins. In Fig. 10 (left), we report the total cross section data and the corresponding curves from step (A). As demonstrated by the plots, our calculation, even without performing any adjustment of the resonance parameters, is able to give a good accounting of the main features of the data in a wide W and Q^2 region. The total cross section strength for $W < 1.65$ GeV (except for the region close to threshold), and for $W > 1.8$ GeV is well reproduced. However, a strong discrepancy is evident at W around 1.7 GeV. Moreover, at this energy the reference curve exhibits a strong peak in the $\pi^+\pi^-$ invariant mass (Fig. 10, right), connected to sizeable ρ meson production. This contribution was traced back to the 70-91% branching ratio of the $P_{13}(1720)$ into this channel [1, 15, 16].

Step (B) - We then considered whether the observed discrepancy around 1.7 GeV could be accommodated by varying the electromagnetic excitation of one or more of the PDG states. In our code, interference effects between continuum and resonances like those reported in Ref. [11], are taken into account automatically inside the model frame [12]. Therefore, our investigation at this stage was including the possibility of accounting for the 1.7 GeV structure via interference effects, although the peaking of such an interference pattern at the same W for all Q^2 bins would be rather surprising. All fit χ^2/ν values were calculated from the 8 W bins between 1.64 and 1.81 GeV and from the 3 Q^2 bins (624 data points). The number of free parameters ranged from 11 to 32, depending on the fit, corresponding to $\nu=613$ to 592 degrees of freedom. Assuming the resonance properties given by the PDG, the bump at about $W=1.7$ GeV cannot be due to the $D_{15}(1675)$, $F_{15}(1680)$, or $D_{33}(1700)$ states; the first because its well known position cannot match the peak; the second because of its well known position and photocouplings [17]; the third due to its large width (~ 300 MeV). The remaining possibilities from the PDG are the $D_{13}(1700)$, the $P_{13}(1720)$, and the $P_{11}(1710)$ (the latter was not included in step (A)), as there are no data avail-

TABLE I: PDG $P_{13}(1720)$ parameters from fit (B) and new state parameters from fit (C). Errors are statistical.

	M (MeV)	Γ (MeV)	$\frac{\Gamma_{\pi\Delta}}{\Gamma}$ (%)	$\frac{\Gamma_{\rho N}}{\Gamma}$ (%)
PDG P_{13} (B)	1725 ± 20	114 ± 19	63 ± 12	19 ± 9
PDG [1]	1650-1750	100-200	N/A	70-85
new P_{13} (C)	1720 ± 20	88 ± 17	41 ± 13	17 ± 10

able on the Q^2 dependence of $A_{1/2}$ or $A_{3/2}$ [17]. If no configuration mixing occurs, the $D_{13}(1700)$ cannot be excited in the SQTm from proton targets, while the SQTm prediction for the $P_{13}(1720)$ relies on ad hoc assumptions. According to the literature [1, 15, 16], hadronic couplings of the $D_{13}(1700)$ and the total width of the $P_{11}(1710)$ are poorly known, while the $P_{13}(1720)$ hadronic parameters should be better established. Several other partial waves were investigated in step (C).

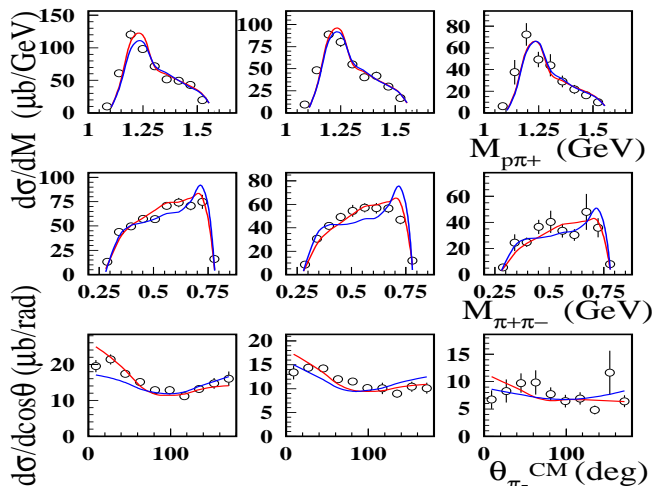


FIG. 11: $\frac{d\sigma_v}{dM_{p\pi^+}}$, $\frac{d\sigma_v}{dM_{\pi^+\pi^-}}$, and $\frac{d\sigma_v}{d\cos\theta_{\pi^-}}$ from CLAS (from top to bottom) at $W=1.7-1.725$ GeV and for the three mentioned Q^2 intervals (left to right). The error bars include statistical errors only. Curves (see text) correspond to the fits (B2) (red), and (B4) (blue), and are extrapolated to the mass distributions edge points.

To improve our reference curves before fitting the bump at around 1.7 GeV, the following steps were carried out: the $P_{11}(1440)$ strength was fitted to our low W data; the $D_{15}(1675)$ and the $D_{13}(1700)$ photocouplings (which vanish in the SQTm) were replaced by NRQM values from Ref. [14]; an empirically established $A_{1/2,3/2}$ SQTm fitting uncertainty or NRQM uncertainty of 10 or 20% (σ) was applied to all N^* states; the hadronic parameters were allowed to vary for the $D_{13}(1700)$ according to Ref. [15]; and finally, the curves providing the best χ^2/ν were selected as the starting points. First we performed three fits, (B1), (B2), and (B3), where the photocouplings of only one resonance at a time were varied. In (B1), we varied $A_{1/2}$, $A_{3/2}$, hadronic couplings, and position of the $D_{13}(1700)$ in a wide range. In (B2), the same was done for the $P_{13}(1720)$, and in (B3) for the

$P_{11}(1710)$. In both fits (B2) and (B3), we also varied the hadronic parameters and the position of the $D_{13}(1700)$ over a range consistent with their large uncertainties from Ref. [15]. Fits (B1) and (B3) gave a poor description of the data, with $\chi^2/\nu=5.2$ and 4.3, respectively. The best fit ($\chi^2/\nu=3.4$) was obtained in (B2) (Fig. 11). However, the resulting values for the branching fractions of the $P_{13}(1720)$ were significantly different from previous analyses reported in the literature and well outside the reported errors [1, 15, 16]. Starting from (B3), we then performed a final fit, (B4), for which the $P_{13}(1720)$ hadronic couplings were fixed from the literature, and varying the photocouplings of all three candidate states, $D_{13}(1700)$, $P_{13}(1720)$, and $P_{11}(1710)$, by 100% (σ). No better solution was found, the χ^2/ν being 4.3 (Fig. 11). In Fig. 12 we report the final comparison of fits (B2) and (B4) with the total cross section data. Table I shows our results

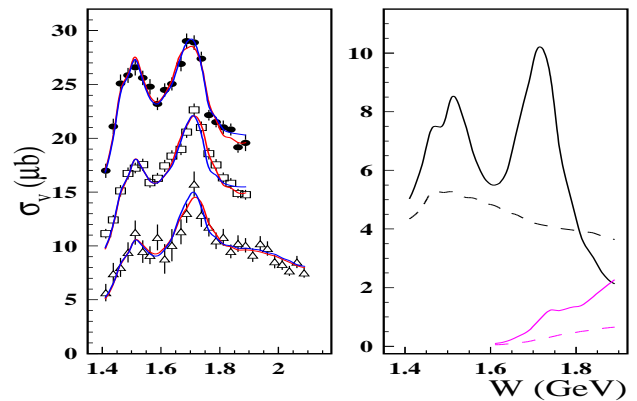


FIG. 12: Left: Total cross section for $\gamma_v p \rightarrow p\pi^+\pi^-$ as a function of W from CLAS at the 3 mentioned Q^2 intervals (see fig.1). The error bars are statistical only. The curves (see text) correspond to the fits (B2) (red), and (B4) (blue). Right: subdivision of the fitted cross section (B2) for $Q^2=0.5-0.8$ (GeV/c) 2 into resonant $\Delta^{++}\pi^-$ (black solid), continuum $\Delta^{++}\pi^-$ (black dashed), resonant $\rho^0 p$ (magenta solid), and continuum $\rho^0 p$ (magenta dashed). Notice the different vertical scales.

(first row) with statistical uncertainties, in comparison with the PDG values (second row). Our fits were not providing an unambiguous separation of $A_{1/2}$, $A_{3/2}$, and the longitudinal $S_{1/2}$, so we report as result the total photocoupling strength, $\sqrt{A_{1/2}^2 + A_{3/2}^2 + S_{1/2}^2}$. The resulting value for the $P_{13}(1720)$ fit is reported in the first three rows of Table II. The errors reflect the statistical uncertainties in the data and the correlations among the different resonances.

As discussed above, fitting the data around 1.7 GeV with established baryon states leads either to a poor fit or to a drastic change in resonance parameters with respect to published results. In the framework of our analysis, there is no way to assess the reliability of the previously determined hadronic parameters of the PDG $P_{13}(1720)$. The resonant content of the reaction $\pi N \rightarrow \pi\pi N$, which is used to obtain the hadronic parameters, may be dif-

TABLE II: PDG $P_{13}(1720)$ total photocoupling from fit (B2) and new state total photocoupling from fit (C). Errors are statistical.

step	Q^2 (GeV/c) ²	$\sqrt{A_{1/2}^2 + A_{3/2}^2 + S_{1/2}^2}$ (10 ⁻³ /√GeV)
B2	0.65	83±5
B2	0.95	63±8
B2	1.30	45±27
C	0.65	76±9
C	0.95	54±7
C	1.30	41±18

ferent from that of reactions initiated by an electromagnetic probe. In particular, the $P_{13}(1720)$ state seen in $\pi N \rightarrow \pi\pi N$ may not be excited in electroproduction, while some other state that decouples from πN may be excited electromagnetically. This possibility is studied in the next step.

Step (C) - We investigated whether our data could be fitted by including another baryon state, while keeping the hadronic parameters of the $P_{13}(1720)$ as in Refs. [1, 15]. The quantum numbers $S_{I1}, P_{I1}, P_{I3}, D_{I3}, D_{I5}, F_{I5}, F_{I7}$ were tested on an equal footing, where $I/2$ is the isospin, undetermined in our measurement. We then simultaneously varied the photocouplings and the hadronic parameters of the new state and the $D_{13}(1700)$. The total decay width of the new state was varied in the range of 40-600 MeV, while its position was varied from 1.68-1.76 GeV. The best fit ($\chi^2/\nu=3.3$) was obtained with a P_{I3} state, while keeping the $P_{13}(1720)$ hadronic parameters at published values. Other partial waves gave a $\chi^2/\nu \geq 4.2$. Curves obtained from the best fit were nearly identical with the red solid lines in Figs. 11 and 12. In order to avoid the unobserved ρ production peak (Fig. 10, right), the photocouplings of the PDG $P_{13}(1720)$ had to be reduced by about a factor of two with respect to the SQTm prediction, making its contribution very small. Instead, in this fit the main contribution to the bump came from the new state. Resonance parameters and total photocoupling value obtained from the assumed new state are reported in Table I (last row) and II (last 3 rows), respectively.

At this point, one could wonder whether a similar discrepancy between the calculation and the data is present in the real photon case, and whether introduction of a new state is compatible with the existing real photon data as well. To this purpose, we reproduce in Fig. 13 the old data from Ref. [18], together with curves obtained from our model. The red solid curve in the graph represents the overall contribution from the non-resonant processes, while the blue dashed line corresponds the resonant contribution only, without introducing any new state. The black dashed line shows the result of our model when including both non-resonant and resonant processes, without new states. Finally, the black solid

curve shows our fit of the real photon data when introducing a new state, and the blue solid curve shows the corresponding modification in the pure resonant excitation curve. The photocouplings of the new $\frac{3}{2}^+(1720)$ state were determined extrapolating the values obtained from the CLAS experiment with virtual photons. An additional adjustment, within 10 %, was applied to reproduce the invariant mass distributions of the pairs $p\pi^+$ and $\pi^+\pi^-$, measured at $W=1.7$ GeV [18]. It is clear how, due to the stronger dominance of the non-resonant mechanisms at the photon point, as well as due to the particular interference effects, a new state can be accommodated into the picture. In fact, the agreement between data and our calculation is even improved by the introduction of the new state.

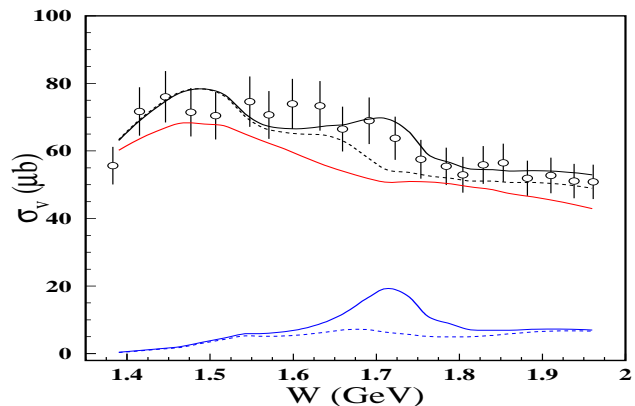


FIG. 13: Total cross section for $\gamma p \rightarrow p\pi^+\pi^-$ as a function of W from Ref. [18], together with curves obtained from our model. Red solid line: overall contribution from the non-resonant processes; blue dashed line: resonant contribution only, without introducing any new state; black dashed line: full calculation, without new states; black solid curve: full calculation, including the new state; blue solid curve: resonant contribution only, including the new state.

A second P_{13} state was indeed predicted in Ref. [4], with a mass of 1870 MeV, and in Ref. [19], with a mass of 1816 MeV. The presence of a new three-quark state with the same quantum numbers as the conventional $P_{13}(1720)$ in the same mass range would likely lead to strong mixing. However, as mentioned above, a different isospin and/or partial wave cannot be excluded. The new state may also have a different internal structure, such as a hybrid baryon with excited glue components. Such a P_{13} hybrid state is predicted in the flux tube model [20]. Finally, in Ref. [21] the existence of a P_{13} pentaquark ($qqqq\bar{q}$) configuration with a mass in the range 1.76-1.78 GeV is predicted. Yet another possibility is that some resonance parameters established in previous analyses may have much larger uncertainties than reported in the literature. In this case, outlined in our step (B), our analysis would establish new, more precise parameters for a known state, and invalidate previous results.

In conclusion, in this paper we presented data on the $ep \rightarrow e'p\pi^+\pi^-$ reaction in a wide kinematic range, with

higher quality than any previous double pion production experiment. Our phenomenological calculations using existing PDG parameters provided a poor agreement with the new data at $W \sim 1700$ MeV. We explored two alternative interpretations of the data. If we dismiss previously established hadronic parameters for the $P_{13}(1720)$ we can fit the data with a state having the same spin/parity/isospin but strongly different hadronic couplings from the PDG state. If, alternatively, we introduce a new state in addition to the PDG state with about the same mass, spin $\frac{3}{2}$, and positive parity, a good fit is obtained for a state having a rather narrow width, a strong $\Delta\pi$ coupling, and a small ρN coupling, while keeping the PDG $P_{13}(1720)$ hadronic parameters at published values. In either case we determined the total photocoupling at $Q^2 > 0$. A simultaneous analysis of single and double-pion processes provides more constraints and may

help discriminate better between alternative interpretations of the observed resonance structure in the CLAS data. Such an effort is currently underway.

We would like to acknowledge the outstanding efforts of the staff of the Accelerator and the Physics Divisions at JLab that made this experiment possible. This work was supported in part by the Istituto Nazionale di Fisica Nucleare, the U.S. Department of Energy and National Science Foundation, the French Commissariat à l'Énergie Atomique, and the Korea Science and Engineering Foundation. U. Thoma acknowledges an “Emmy Noether” grant from the Deutsche Forschungsgemeinschaft. The Southeastern Universities Research Association (SURA) operates the Thomas Jefferson National Accelerator Facility for the United States Department of Energy under contract DE-AC05-84ER40150.

-
- [1] D.E. Groom *et al.*, Eur. Phys. J **C 15**, 1 (2000).
 [2] R. Koniuk and N. Isgur, Phys. Rev. Lett. **44**, 845 (1980); Phys. Rev. **D21**, 1868 (1980).
 [3] M.M. Giannini, Rep. Prog. Phys. **54**, 453 (1991).
 [4] S. Capstick, W. Roberts, Phys. Rev. **D49**, 4570 (1994).
 [5] F. Stancu and P. Stassart, Phys. Rev. **D47**, 2140 (1993).
 [6] M. Kirchbach, Mod.Phys.Lett. **A12**, 3177 (1997).
 [7] E. Smith *et al.*, Nucl. Instr. and Meth. **A432**, 165 (1999).
 [8] B. Mecking *et al.*, accepted for publication in: Nucl. Inst. and Meth. A; W. Brooks, Proc. of PANIC '99, Uppsala, Sweden, 10-16 June 1999, Nucl. Phys. **A 663&664**, 29c (2000).
 [9] E. Amaldi, S. Fubini, and G. Furlan, Pion Electroproduction, Springer Tracts in Modern Physics **83** (1989).
 [10] V. Eckart *et al.*, Nucl. Phys. **B55**, 45 (1973); P. Joos *et al.*, Phys. Lett. **B52**, 481 (1974); K. Wacker *et al.*, Nucl. Phys. **B144**, 269 (1978).
 [11] J.C. Nacher and E. Oset, Nucl. Phys. **A674**, 205 (2000).
 [12] M. Ripani *et al.*, Nucl. Phys. **A672**, 220 (2000); V. Mokeev *et al.*, Phys. of Atomic Nucl. **64**, 1292 (2001); V. Mokeev *et al.*, to be published in Phys. of Atomic Nucl.
 [13] V.D. Burkert, Czech. Journ. of Phys. **46**, 627 (1996).
 [14] F. Close and Z.P. Li, Phys. Rev. **D42**, 2194 (1990).
 [15] D.M. Manley, E.M. Saleski, Phys. Rev. **D45**, 4002 (1992).
 [16] T.P. Vrana *et al.*, Phys. Rept. **328**, 181 (2000).
 [17] V. Burkert, Nucl. Phys. **A684**, 16c (2001).
 [18] ABBHHM collaboration, Phys. Rev. **175**, 1669 (1968).
 [19] M.M. Giannini *et al.*, Eur. Phys. J. **A12**, 447 (2001).
 [20] S. Capstick, P. Page, Phys. Rev. **C66**, 065204 (2002).
 [21] H. Walliser, V.B. Kopeliovich., hep-ph/0304058.